THE JOURNAL OF BIOLOGICAL CHEMISTRY VOL. 287, NO. 6, pp. 4232–4247, February 3, 2012

Single Point Mutation in Bin/Amphiphysin/Rvs (BAR) Sequence of Endophilin Impairs Dimerization, Membrane Shaping, and Src Homology 3 Domain-mediated Partnership*[S]

Received for publication, November 21, 2011 Published, JBC Papers in Press, December 13, 2011, DOI 10.1074/jbc.M111.325837

Anna Gortat[1], **Mabel Jouve San-Roman, Christian Vannier, and Anne A. Schmidt**[2]

From the CNRS, UMR7592, Institut Jacques Monod, Université Paris Diderot, Sorbonne Paris Cité, F-75205 Paris, France

Background: The BAR domain is a dimeric module controlling membrane curvature.
Results: We identify leucine 215 involved in stabilizing the dimer interface and characterize the incidence of its substitution in SH3-mediated partnership in endophilins.
Conclusion: Altered BAR conformation/rigidity impairs membrane binding, shaping, and partnership.
Significance: This mutation in other BAR domain-containing proteins may unravel unanticipated functional relationships between the BAR domain and other structural units.

Bin/Amphiphysin/Rvs (BAR) domain-containing proteins are essential players in the dynamics of intracellular compartments. The BAR domain is an evolutionarily conserved dimeric module characterized by a crescent-shaped structure whose intrinsic curvature, flexibility, and ability to assemble into highly ordered oligomers contribute to inducing the curvature of target membranes. Endophilins, diverging into A and B subgroups, are BAR and SH3 domain-containing proteins. They exert activities in membrane dynamic processes such as endocytosis, autophagy, mitochondrial dynamics, and permeabilization during apoptosis. Here, we report on the involvement of the third α-helix of the endophilin A BAR sequence in dimerization and identify leucine 215 as a key residue within a network of hydrophobic interactions stabilizing the entire BAR dimer interface. With the combination of N-terminal truncation retaining the high dimerization capacity of the third α-helices of endophilin A and leucine 215 substitution by aspartate (L215D), we demonstrate the essential role of BAR sequence-mediated dimerization on SH3 domain partnership. In comparison with wild type, full-length endophilin A2 heterodimers with one protomer bearing the L215D substitution exhibit very significant changes in membrane binding and shaping activities as well as a dramatic decrease of SH3 domain partnership. This suggests that subtle changes in the conformation and/or rigidity of the BAR domain impact both the control of membrane curvature and downstream binding to effectors. Finally, we show that expression, in mammalian cells, of endophilin A2 bearing the L215D substitution impairs the endocytic recycling of transferrin receptors.

The dynamics of intracellular membranes is essential for maintaining the integrity and specialized functions of the eukaryotic cell. This ensures, for example, transport from one compartment to another, adequate sorting of lipids and proteins to organize signaling platforms, and exit from a given compartment. These processes require complex sets of structural and regulatory proteins that control mechanical forces involved in membrane shaping and interplay between membranes and the cytoskeleton.

Bin/Amphiphysin/Rvs (BAR)[3] domain-containing proteins belong to an evolutionarily conserved superfamily of membrane-molding macromolecules, the molecular properties of which have been described relatively recently, driven by ultrastructural analysis by x-ray crystallography, cryo-electron microscopy reconstitution of their assembly on membrane templates, atomic modeling, molecular dynamics simulations, small angle x-ray scattering-based solution studies, and reconstitution of membrane deforming activities *in vitro* (1). The BAR domain superfamily is currently composed of three groups, including the classical BAR whose structure was resolved first (2, 3), the more recently discovered F-BAR (Fes/CIP4 homology BAR), and the I-BAR (inverse-BAR) (1, 4, 5). These three types of domains organize around the interface between two monomers mainly formed by consecutive α-helices that assemble into anti-parallel crescent-shaped dimers whose concave and positively charged face interacts with negatively charged lipid headgroups localized on the cytosolic side of the membrane bilayer. BAR, F-BAR, and I-BAR domains are characterized by more or less curved structures. They can bind to membranes of different curvature degrees with the BAR fitting to the more convex ones (although with relative flexibility, see Ref. 6) and the I-BAR to the more concave ones. In this latter case, for example, the I-BAR is involved in the formation of filopodium-like protrusions (7). All of these domains have been

* This work was supported in part by CNRS, by Grant ACI BCMS 2004 2 421 from the French Ministry of Research, and by grants from the Charities Association pour la Recherche sur le Cancer and La Ligue Nationale Contre le Cancer, Comité de Paris.
[S] This article contains supplemental Figs. 1–9.
[1] Supported by fellowships from CNRS and Association pour la Recherche sur le Cancer.
[2] To whom correspondence should be addressed: CNRS, UMR7592, Institut Jacques Monod, Université Paris Diderot, Sorbonne Paris Cité, Bâtiment Buffon, 15 Rue Hélène Brion, F-75205 Paris, France. Tel.: 33-1-57-27-80-12; Fax: 33-1-57-27-80-26; E-mail: schmidt.anne@ijm.univ-paris-diderot.fr.

[3] The abbreviations used are: BAR, Bin/Amphiphysin/Rvs; EA1, endophilin A1; EA2, endophilin A2; SH3, Src homology 3; Tet, tetracycline; St, StrepTag; PRD, proline-rich domain.

proposed to induce membrane curvature, stabilize curvature driven by other mechanical forces, or sense curvature as a signal for selective recruitment on a given target membrane as well as for the shape-driven attachment to other factors that may act as downstream effectors. Finally, their activity on membranes was also proposed to rely on oligomerization properties that propagate positive curvature to shape tubular structures, as exemplified by self-assembly of F-BAR modules into a helical coat (4).

Among the BAR domain superfamily, the classical BAR sometimes harbors at its N terminus a sequence of ~25 residues that was shown to fold into an amphipathic α-helix upon insertion into the cytosolic leaflet of the membrane bilayer (thus defined as the N-BAR). This is the case of proteins such as amphiphysins, endophilins, and nadrins (1). This helix was proposed to cause membrane bending by pushing apart polar headgroups of lipids from the cytosolic leaflet (8–10) and to contribute to membrane curvature sensing (11, 12). Finally, the N-BAR of endophilins and nadrins was shown to possess a further increased capacity for membrane bending, due to the insertion of an additional membrane-intercalating helix localized in the middle of the first α-helix of the BAR sequence (9, 10, 13, 14).

Endophilins diverge into two groups referred to as endophilins A and B that are composed of a series of three α-helices forming the BAR secondary structure flanked by an N-terminal peptide folding into an amphipathic helix and a C-terminal SH3 domain (for a comprehensive recent review, see Ref. 15). In mammals, endophilins A and B are encoded by three and two genes, respectively, giving rise to endophilins A1, A2, and A3 and endophilins B1 and B2 (16–23). Endophilin A members have mainly been reported as playing roles in endocytosis, in particular in the formation of endocytic vesicles such as synaptic vesicles as historically described (18, 19, 24–30). Endophilin B members appear to have more pleiotropic functions. Endophilin B1, in particular, has been shown to act in endocytosis (31), to control the morphology of mitochondria (32) and their permeabilization during apoptosis (in this context, it was initially named Bif-1 for Bax-interacting factor-1, see Refs. 22, 33–35), to control *de novo* assembly/elongation of autophagic membranes (36), and to act in the formation of Golgi-derived vesicles. In this latter case, it was shown to exert interchangeable functions with CtBP/BARS-50 involved in the fission of COPI-coated vesicles (37). Importantly, endophilins differ from many other BAR domain-containing proteins because their BAR module is not directly flanked by a lipid-binding domain mediating selective membrane recruitment driven by lipid-signaling activity.

Although high resolution structures of the BAR domain of endophilin A1 (9, 10, 13) and of the SH3 domain of endophilin A2 were resolved (38), this is not the case for full-length proteins. Thus, structural and functional relationships between SH3 and BAR domains of endophilin have been poorly investigated. However, modeling using small angle x-ray scattering led to the proposal of a structural relationship involving physical contact between these domains (6). In particular, it was proposed that when the BAR monomers are assembled into a dimer to constitute the so-called BAR domain, the C-terminal SH3 domain folds back toward the distal tip of the adjacent protomer. This interaction, involving a series of positively charged residues located between the second and the third helices of the BAR monomer, could serve the purpose of regulating the interaction with target membranes, as was proposed for the F-BAR-containing protein syndapin (39).

Here, using the combination of N-terminal truncations and single point mutagenesis in proteins of the endophilin A subfamily, we bring converging biochemical evidence for a functional relationship between BAR sequence dimerization and SH3 domain-mediated partnership. We identify leucine 215 as playing a central role in stabilizing hydrophobic interactions between BAR protomers and characterize the impaired activities of the BAR domain of endophilin A2 bearing the L215D substitution in membrane deformation, partnership of the SH3 domain, and endocytic recycling of the transferrin receptor.

EXPERIMENTAL PROCEDURES

Cloning and Mutagenesis—cDNAs encoding for mouse EA1 and the deletion mutants EA1Δ(1–97), EA1Δ(1–175), EA1Δ(1–200), and EA1varSH3 were amplified using sense and antisense primers designed to contain BamHI restriction sites for cloning into the bacterial pET9a expression vector (Novagen). EA1(1/2var)SH3 and EA1SH3 were cloned into pET9a using primers introducing a sequence encoding for a StrepTag in the N terminus and containing NdeI/BamHI restriction sites. The sequences of primers bearing StrepTag insertions were as follows: EA1(1/2var)SH3 sense (5′–3′), GGGAATTCCATATGGCTAGCTGGAGCCACCCGCAGTTCGAAAAAATCGAAGGGCGCAGTACTCAGCCCAACGGGGGTCTC; EA1SH3 sense (5′–3′), GGGAATTCCATATGGCTAGCTGGAGCCACCCGCAGTTCGAAAAAATCGAAGGGCGCGGTGTCCAAATGGATCAGCCCTGC; and EA1(1/2var)SH3 and EA1SH3 antisense (5′–3′), CGGGATCCCTAATGGGGCAGAGCAACCAGAATTTC.

The single point substitutions L215D in the sequences encoding for EA1 and EA2 were obtained by two-step PCRs using the following primers containing silent mutations for screening: EA1LD sense (5′–3′), CTCCTCGAGATGGATATAGAACAGGTGAGCCAGGACTCCGCAC; EA1LD antisense (5′–3′), GGAGTCCTGGCTCACCTGTTCTATATCCATCTCGAGGAGGTTG; EA2LD sense (5′–3′), CTCCTCGAGACTGATATAGAGCAGGTGAGCCAGGACTCGGCCCTGGTGG; and EA2LD antisense (5′–3′), GGCCGAGTCCTGGCTCACCTGCTCTATATCAGTCTCGAGGAGGTTGTGC.

The substitutions of amino acid residues ^{171}KKKR^{174} by ^{171}AAAA^{174} in full-length EA1 was performed by two-step PCRs using the following primers containing silent mutations to generate a NotI restriction site for screening: EA1KA sense (5′–3′), GGTTATGCGGCCGCAGCACAAGGCAAGATTCCAGATGAAGAACTC, and EA1KA antisense (5′–3′), GCCTTGTGCTGCGGCCGCATAACCAAAGTCTAAGCGTCGGCC.

Sequences encoding for full-length EA1, EA1KR and EA1LD, EA1ΔSH3, EA1Δ(1–175), EA1LDΔ(1–175), EA1Δ(1–175)ΔSH3, EA1Δ(1–200)ΔSH3, full-length EA2 and EA2LD, EA2Δ(1–175), EA2LDΔ(1–175), and EA2Δ(1–175)ΔSH3 were

cloned into the pASK3 or pASK7 bacterial expression vectors (IBA, GmbH, Germany), using EcoRI/BamHI restriction sites. Sequences encoding for EA2 and EA2LD were cloned into the eukaryotic pcDNA3.1/myc-His and pcDNA4/TO/myc-His (Invitrogen) and pEXPR-3 and pEXPR-5 (IBA, GmbH, Germany) expression vectors using primers containing BamHI/EcoRI and SacII/BamHI restriction sites, respectively. Sequences encoding for EA2ΔSH3 and EA2LDΔSH3 were also cloned into pEXPR-3 using the same restrictions sites as for full-length sequences.

EA2-mycHis$_6$ was constructed using amplification with sense and antisense primers containing NheI and NotI restriction sites followed by cloning in a modified pET28b expression vector (Novagen), in which sequence NcoI-XhoI was replaced with a NcoI-NheI-NotI-myc-XhoI sequence. This allowed in-frame fusion of EA2 C terminus to the myc tag sequence and the original His$_6$ tag, giving pET2-EA2mh plasmid. Sequence encoding for the ADAM15 cytosolic tail (ADAM15-CT) was cloned into the pGEX-6p-1 vector using primers containing BamHI/XhoI restriction sites. The DNA sequences amplified to obtain the pleckstrin homology and the proline-rich domains of human dynamin 1 (Swiss-Prot accession number Q05193), using primers containing BamHI/XhoI restriction sites for cloning into pASK-3 and BamHI/EcoRI for cloning into PGEX-6p-1, encode for amino acid residues 506–641 and 743–864, respectively.

Expression and Purification of Recombinant Proteins—Recombinant proteins were produced using BL21pLysS bacteria (Invitrogen). Full-length EA1 and BAR-truncated forms were purified by poly-L-proline chromatography, from 280,000 × *g* high speed supernatants obtained from lysed cells as described previously (40). Truncated forms devoid of any BAR sequence fused to a StrepTag and ADAM15-CT fused to GST were purified from high speed supernatants either via StrepTactin/Sepharose or glutathione/Sepharose chromatography according to the manufacturer's instructions (IBA, GmbH, Germany and Amersham Biosciences, respectively). We failed to purify EA1LD and EA2LD mutants because of the total insolubility of both proteins upon expression in BL21pLysS cells. Therefore, we have chosen to express EA2LD as a heterodimer with a wild type version of EA2 bearing a myc-His$_6$ sequence fused at its C terminus. A soluble heterodimer could be expressed in BL21pLys cells transformed with both pASK-3-EA2LD and pET2-EA2mh plasmids and purified by StrepTactin column chromatography as described above. The immunoblot detection of the myc tag in the purified protein confirmed the association of the two polypeptides as a heterodimer.

Protein-Protein Overlay Assays—Rat brain cytosol (~80 μg of total protein per strip, Fig. 5 and supplemental Fig. 4) or ADAM15 fused to GST (0.5 μg, Figs. 1*B* and 5, *bottom panels*) were migrated on SDS-PAGE (10% acrylamide gels). After transfer onto nitrocellulose, membrane strips were incubated for 1 h at room temperature with blocking buffer (TBST-BSA: 150 mM NaCl, 20 mM Tris, 1% (w/v) delipidated BSA, 0,1% (w/v) Tween 20, pH 7.4) and then for 2 h with the indicated proteins in TBST-BSA. These were used under the following conditions: 0.2 μg/ml per strip in Fig. 5 (*top panels, brain cytosol*); 0.5 μg/ml per strip in Fig. 5 (*bottom panel, ADAM15CT*); the indicated amounts in supplemental Fig. 4; dilutions of aliquots of 280,000 × *g* high speed supernatants (Fig. 1*B*) in TBST-BSA containing the equivalent of 3 μg/ml recombinant protein fused to the StrepTag as measured by quantitative analysis of StrepTactin-HRP activity using St-EA1Δ(1–175) purified on StrepTactin/Sepharose and blotted on nitrocellulose as reference. After washing in TBST, the strips were incubated with StrepTactin-HRP in blocking buffer for 30 min at room temperature. After washing, membranes were treated as described under "Immunoblotting."

Sucrose Gradients—Continuous 5–30% (w/v) sucrose gradients were prepared in buffer containing 150 mM NaCl, 25 mM Tris, pH 7.3. 20 μg of the indicated recombinant proteins were loaded on top of 10-ml pre-poured gradients that were subsequently centrifuged for 14 h at 40,000 rpm in a SW41.T1 rotor (Beckman), at 4 °C. Fractions (500 μl each) were collected from top to bottom, and aliquots were subjected to 10% SDS-PAGE. Proteins were detected after transfer onto nitrocellulose, using HRP-conjugated StrepTactin.

Liposome Binding and Chemical Cross-linking—Liposomes were prepared by a slightly modified swelling method as described elsewhere (8). Two binding protocols were used. For endophilin cross-linking experiments, liposomes were prepared from bovine brain lipid extract (Folch fraction I, Sigma) using 2.5 μmol of lipids to yield a 1-ml suspension in PBS. All assays were performed in PBS, in a total volume of 150 μl containing 2.5 μg (≈0.4 μM) of purified recombinant protein and, when required, 0.05 μmol of lipids incorporated into liposomes. All samples were incubated for 20 min at 37 °C. Then the heterobifunctional cross-linking agent 1-ethyl-3-[3-dimethylaminopropyl]carbodiimide hydrochloride from a 50 mM stock in distilled water was added to reach final concentrations of 0, 0.5, and 5 mM. Samples were further incubated for 10 min at 37 °C. Reactions were quickly terminated by adding Laemmli sample buffer and boiling at 95 °C for 5 min. For binding assay, liposomes of defined composition were obtained by mixing (mol %) egg phosphatidylcholine (38), phosphatidylethanolamine (34), liver phosphatidylinositol (5), phosphatidic acid (7.5), phosphatidylserine (8), and cholesterol (7.5). All lipids were from Avanti Polar Lipids and used as a pre-mix in chloroform. A final suspension (1.25 mM lipids) was prepared in HNE buffer (25 mM Hepes, pH 7.4, 0.1 M NaCl, 0.5 mM EDTA) and extruded three times through 0.4-μm (pore size) polycarbonate filters (Avanti Polar Lipids). Binding was carried out in centrifuge polycarbonate tubes by adding liposomes (25 μl, 1.2 or 0.6 mM) to a 2-μM solution of endophilin (25 μl) in HNE buffer, and incubating for 15–20 min at 25 °C. After gentle addition of 100 μl of HNE, the reaction mixtures were centrifuged for 20 min at 250,000 × *g* at 16 °C with the Beckman Coulter TLA 100 rotor. The supernatant was carefully removed, and the pellet was resuspended in HNE buffer. The two fractions were diluted with Laemmli sample buffer. Samples were subjected to SDS-PAGE and analyzed by Western blotting.

Antibodies—The primary antibodies used in immunoblots and immunofluorescence were as follows: rabbit polyclonal anti-endophilin A1 serum raised against an epitope localized at the beginning of the variable region; rabbit polyclonal antiserum raised against a peptide corresponding to the N terminus

of endophilin A members (gift from H.-D. Soeling); mouse monoclonal anti-myc (Cell Signaling); and mouse monoclonal anti-StrepTag II (IBA). Secondary antibodies were as follows: HRP-conjugated AffiniPure goat anti-rabbit (Jackson ImmunoResearch Laboratories Inc.); goat anti-rabbit IgG coupled to Alexa Fluor 568 and chicken anti-mouse IgG coupled to Alexa Fluor 488 (Molecular Probes). Proteins fused to the StrepTag epitope were detected using HRP-conjugated StrepTactin (IBA) according to the manufacturer's instructions.

Immunoblotting—Immunoblotting was performed exactly as described previously (41). Peroxidase activity using either conjugated secondary antibodies or conjugated StrepTactin was detected by enhanced chemiluminescence using the ECL Plus detection kit (GE Healthcare). Images were obtained by direct capture of chemiluminescence using the Intelligent Dark Box LAS-3000 (Fuji, Tokyo, Japan) imaging system and signals quantified using the ImageQuant software.

Immunofluorescence—For immunostaining, HeLa and HeLa/T-Rex cells grown on glass coverslips were rinsed with PBS and fixed with 3% paraformaldehyde for 20 min. All steps were performed at room temperature. Coverslips were rinsed with PBS, and paraformaldehyde was quenched for 20 min using 50 mM NH_4Cl in PBS. After washing with PBS, cells were permeabilized for 10 min in PBS-containing protease inhibitor mixture (Roche Applied Science) and 0.3% (w/v) Triton X-100. Further steps were performed using PBS, 0.2% (w/v) gelatin. Cells were rinsed three times for 30 min and incubated with primary antibodies for 60 min at room temperature. After washing, cells were incubated for 30 min with secondary antibodies. After washing, the coverslips were rapidly soaked into distilled water and mounted in Mowiol or Dako mounting medium (Dako).

Cell Lysis and Co-precipitation Experiments—All steps were performed at 4 °C. Transfected cells in 6-well plates were washed three times with PBS before incubation for 30 min in 300 μl of solubilization buffer (SB: 1% (w/v) Triton X-100, 100 mM NaCl, 2 mM EDTA, 50 mM Tris-HCl, pH 7.4) complemented with protease inhibitor mixture (Roche Applied Science). Cells were then scraped from the dish, and the lysates were incubated for 15 min before centrifugation for 10 min at 900 × *g*. 20 μl of StrepTactin/Sepharose beads pre-washed with SB (IBA GmbH, Germany) were added to 100 μl of the supernatants and incubated for 1 h on a rocking platform. The samples were centrifuged, and supernatants were kept. The beads were washed three times with 500 μl of SB and resuspended to reach the final volume of 35–100 μl. Samples were boiled for 5 min in Laemmli sample buffer, and the solubilized material (referred to as Eluate, E) was subsequently submitted to SDS-PAGE and immunoblotting.

Cell Culture, Transfection and Establishment of Stable Cell Lines—HeLa cells were grown in DMEM (PAA) supplemented with 10% fetal calf serum, 2 mM L-glutamine, and penicillin/streptomycin (PAA) at 37 °C, in 5% CO_2. HeLa/T-Rex cells were grown according to the manufacturer's instructions (Invitrogen).

Cells grown at 60% confluency in 6-well plates (Nunc) were transfected with Lipofectamine 2000 according to manufacturer's instructions (Invitrogen). Cells were used between 16 and 24 h post-transfection.

Establishment of HeLa/T-Rex cell lines that stably express the Tet repressor for tetracycline-inducible expression of EA2LD was performed 48 h after transfection (with the pcDNA4/TO/myc-His plasmid containing the insert encoding for EA2LD) in selection medium containing 0.8 mg/ml Zeocin (Invitrogen). HeLa/T-Rex clones expressing EA2LD in a Tet-inducible manner were grown in minimum Eagle's medium supplemented with 10% fetal calf serum, 2 mM L-glutamine, penicillin/streptomycin, 0.6 mg/ml Zeocin, and 5 mg/ml blasticidin at 37 °C, in 5% CO_2.

Tf-Alexa 568 Uptake—HeLa/T-Rex cells treated or not with tetracycline were washed and incubated for 60 min in DMEM without serum and complemented with 1% BSA (DMEM/BSA). Cells were then washed with the same medium and incubated in DMEM/BSA containing 10 μg/ml Tf-Alexa 568 (Molecular Probes) for 20 min at 37 °C in 5% CO_2. After washing twice in ice-cold PBS, cells were fixed with 3% paraformaldehyde for 45 min on ice and further processed as described under "Immunofluorescence."

Fluorescence Microscopy and Quantitative Analysis of Tf-Alexa 568 Uptake—For qualitative fluorescence microscopy, fluorescence images were acquired under oil immersion ×63 or ×40 objective lenses with ApoTome system composed of an inverted microscope Zeiss Axiovert 200, a camera Axiocam MRm (pixel size 6.45 × 6.45 μm), the Zeiss ApoTome system, and acquisition software Axiovision 4.5. Images were treated with ImageJ and Photoshop software.

For quantitative fluorescence microscopy (see Fig. 9*C*), a Leica Sp5 confocal imaging microscope, equipped with a ×63 oil PlanApo numerical aperture (NA) 1.4 was used. The object was scanned at 400 Hz with a resolution of 512 × 512 × 21 pixels and a voxel size of 0.76 × 0.76 × 0.88 μm. The pinhole was adjusted to fit the airy disc. Alexa Fluor 488 and 568 fluorophores were excited at 488 and 561 nm wavelength, respectively. Emission fluorescence was detected by photomultiplicator between 495 and 560 and 600 and 730 nm. Cross-talk between channels was controlled by scanning cells labeled with a single fluorophore. For quantitative fluorescence analysis, Z-piles of images were treated with Imaris 7.3.1 (BITPLANE) software. Each cell in the field, imaged in its entire volume, was analyzed after hand-controlled definition of its three-dimensional contour (cells in touch with the borders of the field or in tight clusters preventing unambiguous delimitation of contour were systematically discarded). Sum of fluorescence intensities in each channel (integrated in the entire volume and expressed as "three-dimensional sum of fluorescence intensities per cell") were calculated by Imaris. For each cell, individual parameters were exported to Excel and KaleidaGraph softwares for calculation, statistical analysis, and graphics. The threshold above which cells were referred to as "EA2LD-expressing cells" was determined from fluorescence measured in the green channel for cells not treated with Tet. The mean values of background fluorescence in the green channel for "EA2LD-nonexpressing cells," in the (+Tet) and (−Tet) conditions, were relatively comparable (see Fig. 9*C*, *left panels*, for 5 and 16 h ± Tet).

Negative Staining—Carbon Formvar-coated-grids were floated for 6 min on a liposomes plus endophilin mixture (8 μl final volume) prepared as for the binding assay described above.

The excess fluid was removed by touching the edge of the grids to filter paper. The grids were immediately transferred to droplets of 4% uranyl acetate and stained for 3 min. The excess fluid was drawn off with a filter paper, and grids were allowed to air-dry for 10 min before observation at 80 kV in a Tecnai G2 transmission electron microscope.

RESULTS

BAR and SH3 Domains of Endophilin Are Functionally Linked—Endophilin A1 (EA1), one of the three endophilin A members that is highly expressed in brain, was described initially to bind to poly-L-proline immobilized on Sepharose (40). This interaction takes place via its SH3 domain known to interact with several proteins containing proline-rich regions bearing the P*X*RPP or PP*X*RP consensus sequence (42, 43). The binding of full-length recombinant EA1 to poly-L-proline, although of low efficiency, requires the SH3 domain because the SH3-deleted (ΔSH3) form does not interact with poly-L-proline (Fig. 1*A* and see also supplemental Fig. 1 for an overview of all mutant and tagged forms used in this study). Similar behavior was found for the ubiquitously expressed form endophilin A2 (EA2) that binds to poly-L-proline with even lower efficiency (data not shown). Interestingly, while purifying a series of N-terminally truncated forms of EA1 encompassing the three helices of the BAR sequence via binding to immobilized poly-L-proline, we observed that the form devoid of the first α-helix was immobilized with low efficiency (as the full-length protein) but that proteins lacking the two N-terminal helices (EA1Δ(1–175) and EA1Δ(1–200)) could bind much more efficiently (Fig. 1*A*). This interaction with poly-L-proline still takes place via the SH3 domain because the double deleted form EA1Δ(1–200)ΔSH3 was not immobilized (Fig. 1*A*). Surprisingly, none of the deleted forms composed of the SH3 domain (fused or not to half or the entire variable region linking the BAR sequence to the SH3 domain) were found to bind significantly to poly-L-proline (Fig. 1*A*). These discrepancies in the binding of truncated forms of EA1 were confirmed using a *bona fide* proline-rich domain, *i.e.* the cytosolic part of the trans-membrane metalloprotease ADAM15 (ADAM15-CT) known to interact with endophilins (44). Using protein/protein overlay assays, we found that EA1(1/2var)SH3, EA1varSH3, and EA1SH3 bind poorly to the proline-rich region of ADAM15-CT immobilized on nitrocellulose, in comparison with EA1Δ(1–175) (Fig. 1*B*). In addition, it should be specified that the interaction of St-EA1Δ(1–175) with ADAM15-CT takes place via the SH3 domain because its truncation abolished the formation of the complex (see Fig. 5). These results validated the data obtained by poly-L-proline chromatography using a biologically relevant interacting partner.

The discrepancy between polyproline binding of EA1 lacking the first 175 amino acid residues and the full-length protein (or the truncated form lacking the first α-helix) may be explained by at least two possibilities that may not be mutually exclusive. First, the SH3 domain interacts either in the BAR sequence or in the protomer when BAR sequences are assembled as a dimer or intermolecular interaction with the adjacent protomer in the BAR domain. Second, the high polyproline

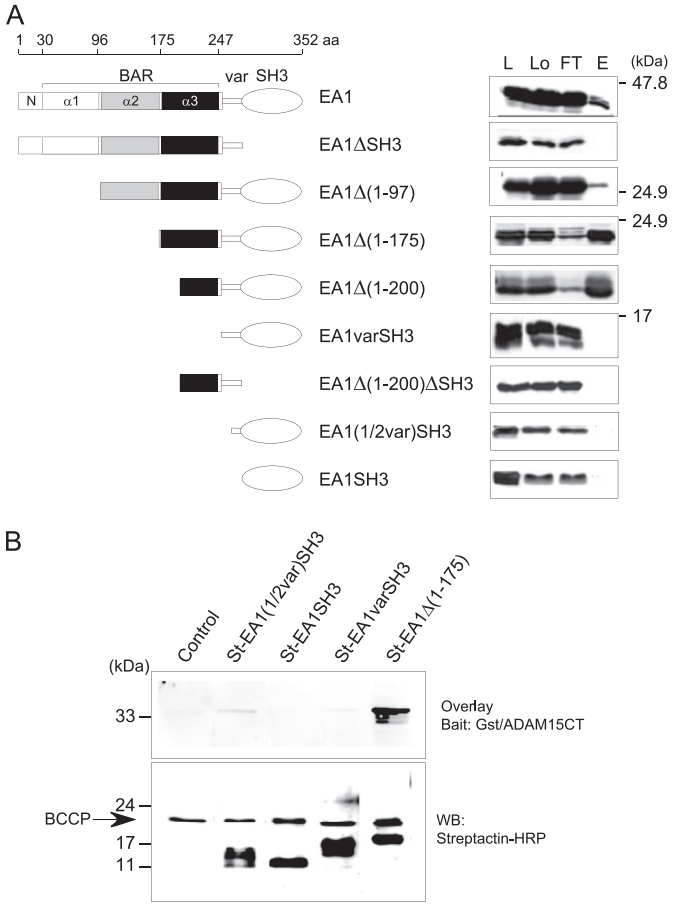

FIGURE 1. **Differential binding of EA1 and truncated forms to proline-rich peptides.** *A, left,* rod structure of full-length EA1 and truncations (Δ) encompassing the SH3 domain and/or the first, second, and third helices (α1, α2, and α3, respectively) of the BAR sequence as well as half (EA1(1/2var)SH3) or the entire (EA1varSH3) variable region (*var*). Note that α1 is broken by a peptide sequence that folds into a central amphipathic helix that is not depicted here (residues 63–86). *Right,* binding of full-length and truncated forms on poly-L-proline/Sepharose. Lysates (*L*) from bacteria were centrifuged, and supernatants were loaded (*Lo*) onto poly-L-proline/Sepharose columns for affinity chromatography. Samples from the lysates and equal proportions of samples from the load, the flow-through (*Ft*), and the eluted proteins (*E*) were run on SDS-PAGE and analyzed for protein content by Western blotting using an anti-EA1 polyclonal antiserum or StrepTactin-HRP recognizing the N-terminal StrepTag (for EA1(1/2var)SH3 and EA1SH3). aa, amino acids. *B,* cytosolic tail of ADAM15 fused to GST (GST/ADAM15-CT) was used as bait to recruit the indicated truncated forms of EA1 fused to an N-terminal StrepTag using protein/protein overlay assays. After SDS-PAGE and transfer of GST/ADAM15-CT on nitrocellulose membrane, individual strips were incubated in the presence of high speed supernatants from bacteria containing, or not (control), the equivalent of 3 μg/ml of the indicated EA1 fragments fused to a StrepTag (*St*). *Top panel,* protein complexes on nitrocellulose were revealed using StrepTactin-HRP. *Bottom panel,* aliquots of equal volume of the high speed supernatants diluted in TBST-BSA and used for incubation with the membranes were analyzed for their content in EA1 truncated forms by Western blot (*WB*) using StrepTactin-HRP. Note the presence in the high speed supernatants of the bacterial biotin-carboxyl carrier protein (22.5 kDa), which is recognized by StrepTactin-HRP. The volume of the high speed supernatant used for the control incubation obtained from bacteria transformed with empty plasmid was adjusted to the content in biotin-carboxyl carrier protein of the other samples.

binding capacity of EA1Δ(1–175) relies on its increased ability to dimerize, a hypothesis raised by the fact that the third α-helix of the BAR sequence (α3) contains residues involved in dimerization (13), which is also consistent with the poor interaction of the polypeptides composed of the SH3 domain (with or without the variable region), with poly-L-proline, or ADAM15-CT (Fig. 1).

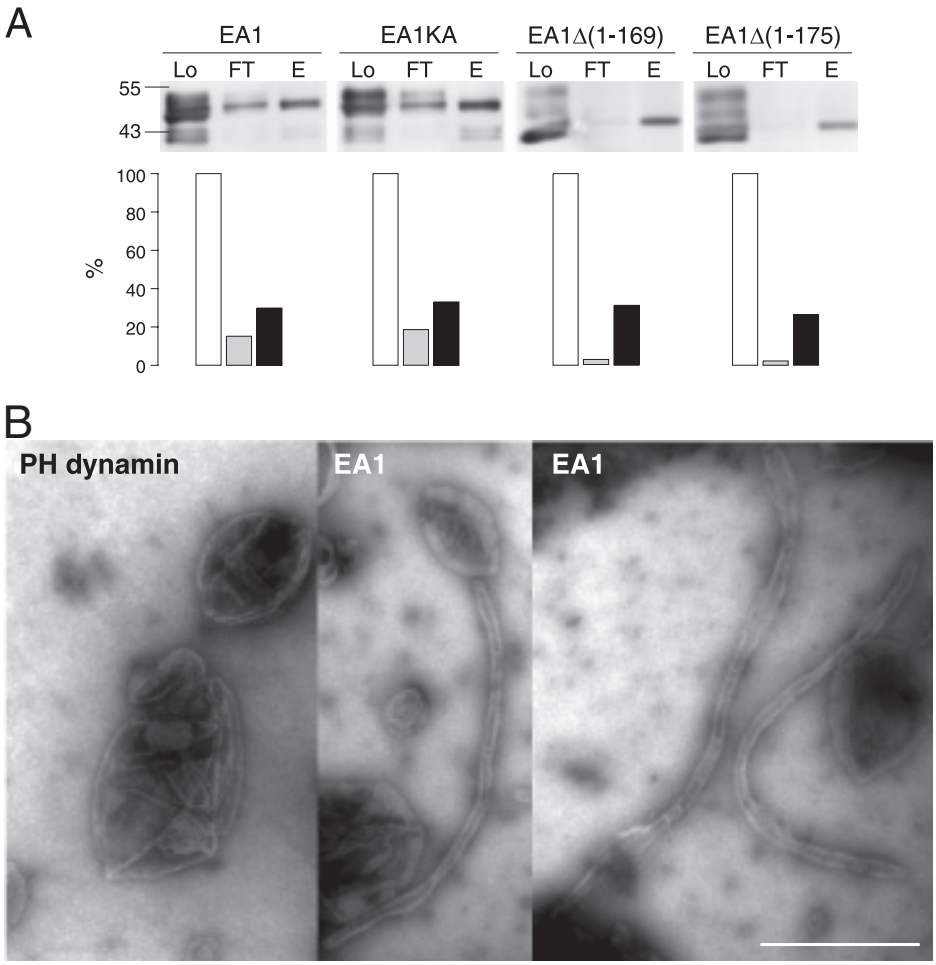

FIGURE 2. **KKKR tetrapeptide in EA1 does not control SH3-mediated partnership.** *A,* SDS-PAGE-Western blot analysis of full-length EA1 and the EA1KA, EA1Δ(1–169), and EA1Δ(1–175) mutants binding to poly-L-proline. Recombinant endophilins (2 μM final concentration) were incubated with poly-L-proline-coupled beads. Fractions are defined as in Fig. 1*A* (*Lo, FT*). Bound material was eluted with 50% DMSO in PBS (*E*). After electrotransfer, proteins were revealed (*upper panel*) with StrepTactin-HRP for quantification. Results expressed (*lower panel*) as a percentage of the amount of loaded protein reveal similar binding behavior for the wild type and mutant endophilins. *B,* negative stain EM of liposomes following incubation with EA1. Binding results in the formation of tubules (30–35 nm in diameter), absent after incubation with the pleckstrin homology (*PH*) domain of dynamin taken as control. *Bar,* 500 nm.

The first possibility is consistent with recent data suggesting that the SH3 domain undergoes electrostatic interaction with the distal tip of the adjacent protomer in the same BAR domain via a positively charged stretch of amino acid residues (^{171}KKKR^{174}) that is located between α2 and α3 in EA1 and is partly conserved in syndapin and amphiphysin (39). To address this point, we compared the respective poly-L-proline binding efficiencies of the following: (i) wild type EA1 and a mutant in which the KKKR peptide was mutagenized in AAAA (EA1KA); (ii) EA1Δ(1–175) and EA1Δ(1–169), the latter containing the N-terminal extension of six amino acid residues that encompasses the ^{171}KKKR^{174} peptide. The loss of positive charges in the EA1KA mutant did not trigger an increase in poly-L-proline binding (Fig. 2*A*, *left,* note the comparable levels of detection of wild type and mutant in the respective flow-through and eluates). In addition, the presence of the KKKR peptide in EA1Δ(1–169) did not hamper the binding efficiency observed with EA1Δ(1–175) (Fig. 2*A*, *right,* note the virtual absence of detection of both deletion mutants in flow-through and the similar levels in eluates). Opposite results should have been expected from an interaction of reasonable affinity between the SH3 domain and the KKKR peptide. Thus, in the particular case of endophilin and in our conditions, this interaction does not have a significant incidence on the accessibility of the SH3 domain. As proposed for syndapin (39), the interaction between the KKMK peptide and the SH3 domain might regulate the interaction of the BAR domain of the protein with membranes. Full-length syndapin, however, has little efficiency in tubulating membranes, but a deletion of the SH3 domain fully restored this activity (39). We found that full-length EA1 incubated in the presence of liposomes was able to generate long tubular structures (Fig. 2*B*). This shows that the putative masking by the SH3 domain of the KKKR peptide (which we can confirm is involved in the interaction of EA1 with target membranes, see supplemental Fig. 2) is of little incidence on the tubulating activity of EA1.

The second possibility that the high polyproline binding efficiency of EA1Δ(1–175) (in comparison with the full-length protein) relies on increased ability to dimerize is supported by experiments using chemical cross-linking, which demonstrated that EA1Δ(1–175) indeed forms dimers (Fig. 3). Interestingly, the formation of EA1Δ(1–175) dimers in solution

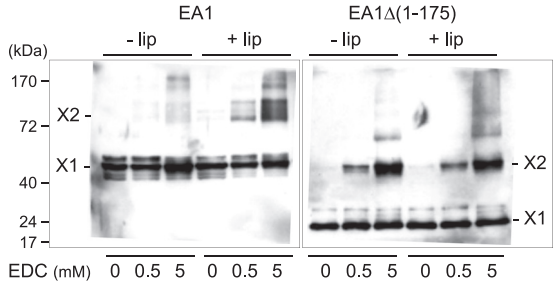

FIGURE 3. **Deletion of the two N-terminal helices of the BAR sequence does not impair dimerization.** Full-length EA1 and (EA1Δ(1–175)) were incubated in the absence (−*lip*) or the presence of liposomes (+*lip*) obtained from bovine brain lipid extract. At the end of the incubation period, the chemical cross-linker 1-ethyl-3-[3-dimethylaminopropyl]carbodiimide hydrochloride (*EDC*) was added or not to reach the indicated final concentrations. Samples were subsequently analyzed by Western blotting to test the capacity of the proteins to form oligomers. *X1,* monomers; *X2,* dimers.

could be detected at a cross-linker concentration lower than for the full-length protein suggesting that EA1Δ(1–175) dimerizes more efficiently (Fig. 3, compare the conditions: liposomes, 0.5 mM 1-ethyl-3-[3-dimethylaminopropyl]carbodiimide hydrochloride). In addition, when the reactions were performed in the presence of membranes, the dimerization of EA1Δ(1–175) was not increased, whereas that of the full-length protein was significantly improved. This suggests that, upon membrane binding, the full-length protein undergoes a conformational change that stabilizes the interaction between protomers. Here, we make the hypothesis that the conformation of the α3-helices in the dimer formed by EA1Δ(1–175) is acquired in full-length EA1 subsequently to a conformational change imposed by lipids on the other two helices of the BAR domain. Finally, the hypothesis that the apparent affinities for proline-rich peptides of deleted and full-length forms are linked to the dimerization is consistent with the observation that the fusion of SH3 domain of endophilin to GST (GST/SH3) triggers a quite significant increase in the efficiency of interaction with poly-L-proline (see supplemental Fig. 3). The interaction of GST/SH3 with poly-L-proline requires the SH3 domain because it does not occur for GST alone (which itself exists as dimers (45)). We believe that the most reasonable explanation for this is that GST/SH3 interacts with poly-L-proline because of forced dimerization via GST.

Altogether, in agreement with data from the EA1 crystal structure (13), our results show that α3 contains critical amino acid residues involved in stabilizing homodimerization. In addition, they strongly suggest that dimerization of BAR monomers drastically increases the affinity/avidity of proline-rich-containing partners with the SH3 domain.

Single Point Mutation in the Third Helix of the BAR Sequence Impairs Dimerization—To bring further evidence on the control by BAR-mediated dimerization of SH3-dependent partnership, we searched for single amino acid substitution impairing dimerization. As we found that α3 contains residues involved in dimerization, we focused on residues in this region that are conserved through species and involved in contact sites between monomers (Fig. 4*A*) (13). In addition, because of the observed correlation between dimerization of EA1Δ(1–175) and a high poly-L-proline binding efficiency, a decrease in binding was used to identify mutations potentially impairing dimerization of this particular deleted form. The two most hydrophobic residues, namely leucines 215 and 233, were substituted by an aspartate (L215D and L233D, respectively). EA1Δ(1–175) bearing the L233D substitution precipitated in high speed supernatants performed before loading on poly-L-proline columns, indicating its tendency to aggregate (data not shown). EA1Δ(1–175) bearing the L215D substitution (EA1LDΔ(1–175)) was soluble and, importantly, unable to bind to poly-L-proline (Fig. 4*B*). To be able to purify EA1LDΔ(1–175), the protein was produced fused to a C-terminal StrepTag, followed by purification using StrepTactin/Sepharose (Fig. 4*B*). As shown by chemical cross-linking (Fig. 4*C*) as well as rate-zonal centrifugation (Fig. 4*D*), EA1LDΔ(1–175) did not dimerize and, accordingly, had a lower sedimentation velocity, in comparison with EA1Δ(1–175).

Altogether, these data are fully consistent with our initial prediction on a positive link between dimerization and poly-L-proline binding efficiency. This suggests that dimerization significantly increases the affinity/avidity for partners of the SH3 domain.

Impairment in BAR Sequence Dimerization Alters Partnership—The extent to which the L215D substitution might impair the association with partners was tested. This was performed using overlay assays with proteins from brain cytosol transferred on nitrocellulose and subsequent probing with deleted forms of EA1 bearing or not the L215D substitution. To generalize the impact of this mutation on the assembly of the BAR domain in other members of the endophilin A subfamily, these experiments were also performed with the ubiquitously expressed form, namely endophilin A2 (EA2). Remarkably, for either EA1 or EA2, the L215D substitution severely impaired the binding to well characterized cytosolic partners of endophilins present in brain cytosol, *i.e.* dynamin and synaptojanin (Fig. 5 and supplemental Fig. 4). In addition and consistently with data shown in Fig. 1*B*, both EA1 and EA2Δ(1–175)-truncated forms interacted strongly with ADAM15-CT. These interactions occur via their respective SH3 domain because, for both proteins, deletion of this domain almost totally abolished the formation of complexes with ADAM15-CT. Finally, the L215D substitution triggered a quite significant decrease of interaction with ADAM15-CT, in agreement with what was observed for the partners from brain cytosol (Fig. 5).

Substitution of Leucine 215 Triggers Alteration in Membrane Tubulating Activity of EA2—To characterize further the incidence of the L215D substitution on membrane binding and membrane deforming activities of endophilin A members *in vitro*, recombinant endophilins A1 and A2 bearing the mutation were produced in bacteria. Unfortunately, neither EA1LD nor EA2LD could be obtained in sufficient amounts (the two mutant proteins precipitated during the high speed pre-clearing centrifugation step that was performed to obtain the material loaded on the column for affinity chromatography, data not shown). To circumvent these problems, we took advantage of the fact that the L215D mutant can interact with sufficient affinity with its wild type counterpart (such a heterodimer is characterized by a lower affinity between protomers as compared with that of wild type ones, see Fig. 8). Because ultimately the aim was to extend observations made *in vitro* on potential

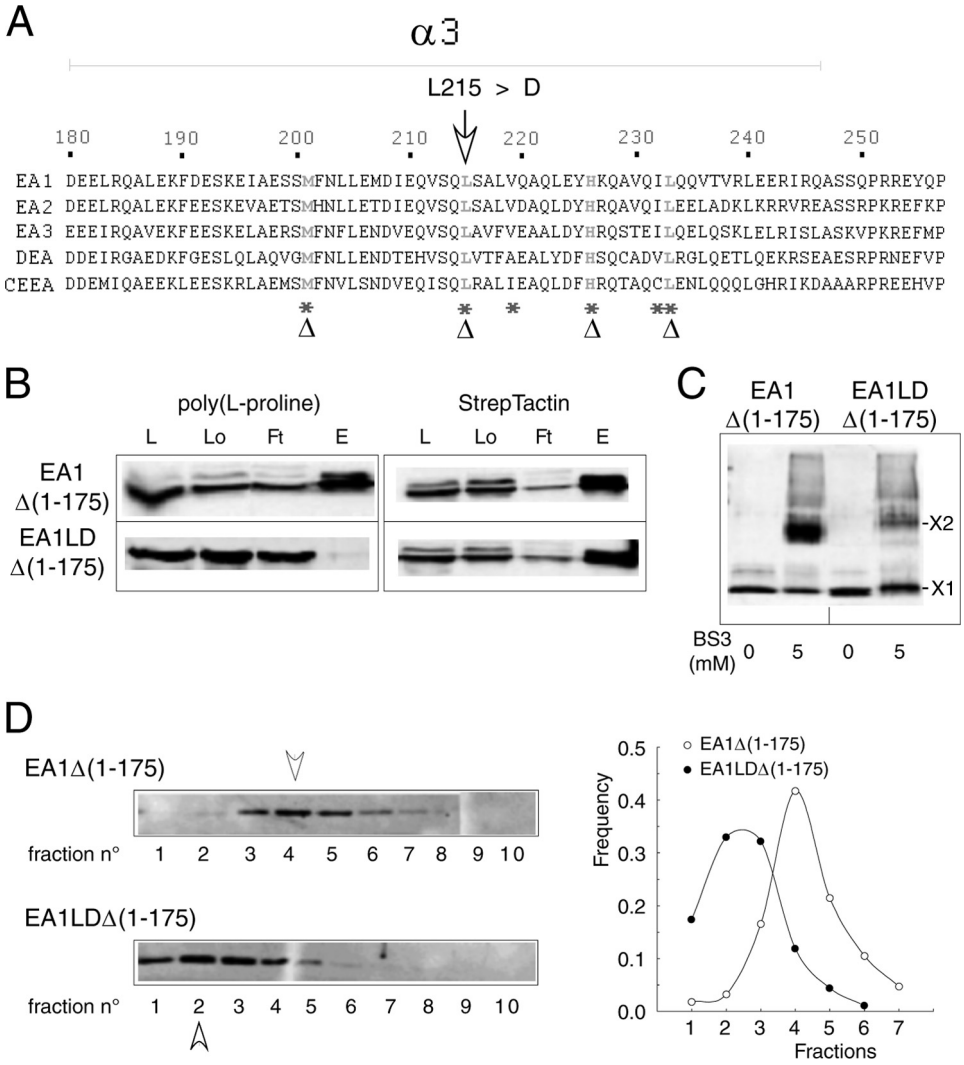

FIGURE 4. **Single point mutation in α3 impairs dimerization.** *A,* structure-based sequence alignment of BAR sequence α3 of endophilin A members through species. EA1, EA2, and EA3 are mouse endophilins A1, A2, and A3 sequences (SwissProt accession number Q62420, Q62419, and Q62421 respectively); *DEA* corresponds to *Drosophila* endophilin A (SwissProt accession number Q8T390); *CEEA* corresponds to *Caenorhabditis elegans* endophilin A (WormBase accession number CE37042). Residues in *gray* and pointed by *triangles* (see text) are conserved through species and have been subjected to mutagenesis. Residues pointed by *asterisks* are involved in dimerization (13). *B,* substitution of leucine 215 impairs binding to poly-L-proline. Lysates obtained from bacteria expressing EA1Δ(1–175) or the corresponding form bearing the L215D substitution (EA1LDΔ(1–175)) were tested for their ability to interact with poly-L-proline as in Fig. 1*A* or purified on StrepTactin/Sepharose. *L*, lysate; *Lo*, load; *Ft*, flow-through; *E*, eluate. *C* and *D,* substitution of leucine 215 impairs dimerization. Proteins purified on StrepTactin/Sepharose were incubated with the indicated concentrations of the chemical cross-linker BS3. Monomers (*X1*) and dimers (*X2*) were detected after SDS-PAGE and blotting with StrepTactin-HRP (*C*) or subjected to ultracentrifugation on sucrose gradient ((*D*) *fraction 1*; top of the gradient). *Arrowheads* indicate the shift in sedimentation coefficients and the fractions at which the highest signals were detected (see quantification of ECL signals on the *right*).

deficiencies of the L215D substitution in the activity of endophilin A members in cells in culture, we focused on EA2, which is ubiquitously expressed. EA2 and EA2LD were produced in doubly transformed BL21 cells, and using a purification protocol primarily based on immobilization of the mutant (tagged with the StrepTag sequence), a heterodimer with the wild type protein (tagged with the myc sequence) could be isolated. When the mutant heterodimer (EA2LD/WT) was incubated with liposomes of relatively homogeneous size and defined lipid composition (see "Experimental Procedures"), both wild type and mutant forms were sedimented in a membrane-dependent manner with a greater efficiency than in the condition where wild type EA2 alone was used (Fig. 6*A*, note the minor fraction of proteins sedimented in the absence of liposomes (*bottom panel*) and compare the efficiencies of precipitation in conditions where EA2 and EA2LD/WT were incubated with 0.6 mM liposomes, top panel and quantifications). These results strongly suggest that the mutant heterodimer has a higher propensity to interact with membranes and, perhaps, to remain associated with them with a longer half-life (see under "Discussion" for more details).

It should be noticed that if more than half the amount of EA2LD interacted with membranes, the unbound pool that was found in the supernatant of the incubation is, most probably and in its majority, a monomer (which results from re-equilibration of the heterodimers obtained after purification toward distinct populations of heterodimers, homodimers, and monomers, consistently with the mass action law and the decreased affinity of EA2LD for its cognate partner). In the case of EA2, a minor population of proteins remained soluble, most probably

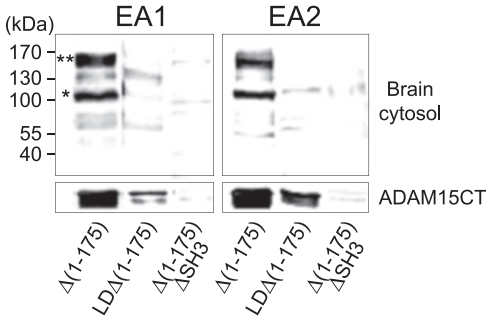

FIGURE 5. **Dimerization is required for SH3 domain-mediated partnership.** EA1 and EA2 with the indicated deletions (Δ(1–175) and Δ(1–175)ΔSH3), either combined or not with the L215D substitution, were assayed for the ability to recognize SH3 domain binding partners from brain cytosol (*top panels*) or purified ADAM15-CT (*bottom panels*) using protein/protein overlay assays. In the *top panels*, both EA1Δ(1–175) and EA2Δ(1–175) bind to dynamin (~100 kDa (*), the presence of which was confirmed by separate immunoblotting (not shown)) and to synaptojanin (~145 kDa (**)).

because the equilibrium favors the dimeric state that became competent for binding to membranes. Altogether, these observations are consistent with a decreased ability of full-length mutant monomers to form stable dimers.

Upon incubation with liposomes, EA2LD/WT triggered the formation of structures visualized by negative staining in electron microscopy morphologically different from those formed in the presence of wild type EA2 (Fig. 6*B*). Detailed analysis of images revealed (for more details, quantification, and statistics, see supplemental Figs. 5 and 6) the following: (i) the obvious heterogeneity in diameter of the tubes that were formed, ranging from very narrow constrictions to large varicosities; (ii) the formation of clusters of spheres with variable diameters; and (iii) the very significant increase in the formation of little particles of significantly smaller size. Neither tubular structures nor free vesicles were observed in control conditions using the pleckstrin homology domain of dynamin as a membrane-binding protein. Altogether, these data clearly show that the L215D substitution modifies the membrane binding and membrane deforming activities of EA2.

EA2LD/WT Heterodimer Is Impaired in SH3 Domain-mediated Partnership—The incidence of the L215D substitution on the binding of partners of the SH3 domain was also investigated. This was addressed in the presence of liposomes, using wild type EA1, EA2, the EA2LD/WT heterodimer, and the PRD of dynamin fused to GST (GST-PRD) as partner (Fig. 7). In agreement with data from Fig. 6, the results confirm the increased ability of the heterodimer to interact with membranes. However, although membrane-bound EA1 and EA2 interacted efficiently with GST-PRD, binding of GST-PRD to membrane-bound heterodimers was very significantly reduced (see the quantitative analysis and the small ratio GST-PRD/EA when the assay was performed in the presence of the EA2LD/WT heterodimer). These results show that the mutation, even limited to one protomer in the dimer, dramatically reduces the binding of partners to a level below the expected capacity of a single protomer in the EA2 homodimer (as attested by the PRD to endophilin ratio in the liposome fraction). These results suggest that this dramatic decrease in affinity for the GST-PRD results from a lower affinity between protomers in the heterodimer possibly associated with modification in the conformation of the C terminus of the BAR domain (the closest in distance to the SH3 domains) and that affects SH3-mediated partnership in both the wild type and the mutant protomers.

Leucine 215 Is Essential for Full-length BAR Sequence Dimerization of Endophilin in Cells—We then addressed the incidence of the L215D substitution on the dimerization property of the full-length BAR sequence and of cellular functions of EA2 in mammalian cells (EA2 is the endophilin A member that appears to be expressed at the highest level in HeLa cells (see supplemental Fig. 7)). We first determined whether transiently expressed wild type EA2 interacts with the endogenous form expressed in HeLa cells (Fig. 8*A*). It should be noticed that with the use of an antibody that recognizes the conserved N-terminal part of all endophilin A members, a major and a minor band having molecular weights in the range expected for EA2 were detected in cells transfected with empty plasmid (Fig. 8*A*, *top left panels*). RNA interference triggered the proportional disappearance of both bands, strongly suggesting that the two proteins are EA2 with the upper form bearing a post-translational modification (see supplemental Fig. 7). To visualize the interaction between endogenous EA2 and transiently expressed forms, cells were transfected with plasmids encoding for EA2 fused at either its N or C terminus with a StrepTag (St). Analysis of material eluted from StrepTactin/Sepharose shows that irrespective of the position of the tag, newly synthesized EA2-St or St-EA2 did not co-precipitate detectable amounts of endogenous EA2 (Fig. 8*A*). This could be due to the fact that mouse and not human EA2 was expressed, suggesting that EA2 monomers from both species cannot interact. However, this is of little probability because only 7 residues of over 240 encompassing the N-BAR sequence differ between both species, with 6 being conserved on the basis of charge or hydrophobicity. In addition, all residues in the third helix predicted to be involved in dimerization are conserved (13). Alternatively, the dimerization of BAR monomers may take place rapidly after biosynthesis, consistent with the existence of a predominant pool of cytosolic EA2 assembled as dimers (46).

To circumvent these potential biases, both myc and St fusions that can be discriminated on the basis of their respective molecular weight were co-expressed in HeLa cells (Fig. 8*B*). Eluates from StrepTactin/Sepharose showed that the two epitope-tagged forms of EA2 can co-precipitate with an apparent ratio close to stoichiometry. This is consistent with the previously formulated hypothesis according to which BAR dimers form rapidly after protein synthesis in mammalian cells (Fig. 8*B*, *top right panels*). When EA2-myc and EA2LD-St were co-expressed in HeLa cells, the two proteins co-precipitated much less efficiently than EA2-myc and EA2-St monomers (Fig. 8*B*, *bottom left panels*). Finally, a barely detectable amount of EA2LD-myc could be precipitated with St-EA2LD upon co-expression (Fig. 8*B*, *bottom right panels*).

Quantification of binding was carried out using co-expression of full-length and SH3-deleted forms, taking advantage of the fact that the latter ones are expressed at a higher level than the full-length forms (in particular for the proteins bearing the L215D substitution). In addition, the lower

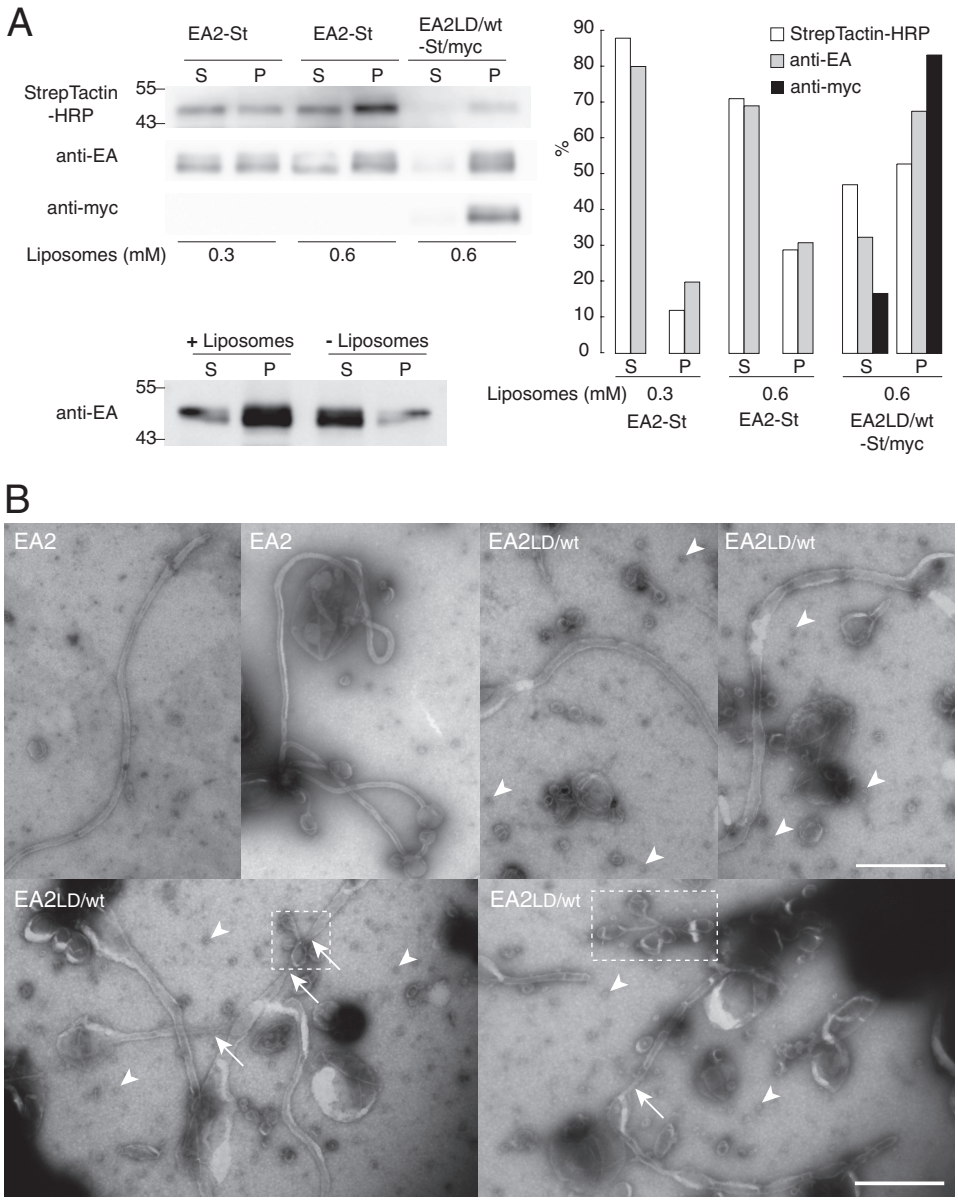

FIGURE 6. **L215D substitution in EA2 does not prevent binding to liposomes but triggers the formation of altered membrane structures.** *A,* liposome binding assay was performed as in Fig. 2*B* by incubating liposomes (0.3 or 0.6 mM total phospholipids as indicated) with either EA2 or the heterodimer EA2LD/EA2 (EA2LD/WT). This dimer was obtained as described under "Experimental Procedures" and harbors a StrepTag (EA2LD protomer) and a myc tag (wild type protomer). Detection of the tags and of endophilin immunoreactivity after electrotransfer (*left, upper panel*) was performed using StrepTactin-HRP, anti-myc and anti-EA antibodies, respectively, for unbound (*S*) and liposome-bound (*P*) fractions. ECL signals were quantified (*right*). Results are expressed as a percentage of the total recovered material in each condition. Note the presence of the mutant protomer in the liposome fraction and the higher binding ability of EA2LD/WT as compared with EA2. Note the very different partitioning of EA2LD/WT between *S* and *P* when the heterodimer was incubated either in the presence or in the absence of liposomes (0.3 mM), with 58 and 4% of the input material recovered in the pellet, respectively. *B,* negative stain EM of liposomes after exposure to EA2 or to EA2LD/WT showing, in the latter case, formation of higher diameter tubes with constrictions (*arrows*) and of numerous small particles (*arrowheads*). Clusters of spheres (*rectangles*) were abundantly formed in the presence of EA2LD/WT (also see supplemental Fig. 5). *Bar,* 500 nm.

molecular weight of these deleted proteins allowed a clear separation from endogenous EA2 upon SDS-PAGE, thus facilitating background subtraction and reliable quantification (see Fig. 8*C* and supplemental Fig. 8). It should be noticed that EA2ΔSH3-St could not co-precipitate detectable amounts of endogenous EA2 (see supplemental Fig. 8), consistently with what was observed with full-length EA2. This indicates that the lack of interaction is not due to an intramolecular regulation of dimerization by the SH3 domain, in particular when monomers are not synthesized concomitantly.

Calculation of the ratio of myc to StrepTag forms in both cell lysates and StrepTactin/Sepharose eluates obtained from HeLa cells co-expressing either EA2 and EA2ΔSH3, EA2 and EA2LDΔSH3, or EA2LD and EA2LDΔSH3 showed a progressive decrease in co-precipitation efficiencies with the most important amplitude for dimers made of cognate L215D protomers (Fig. 8*D*).

Altogether, these data show that the L215D substitution impairs dimerization of full-length BAR monomers. These results are in complete agreement with molecular modeling extrapolated from the crystal structure of EA1, which clearly

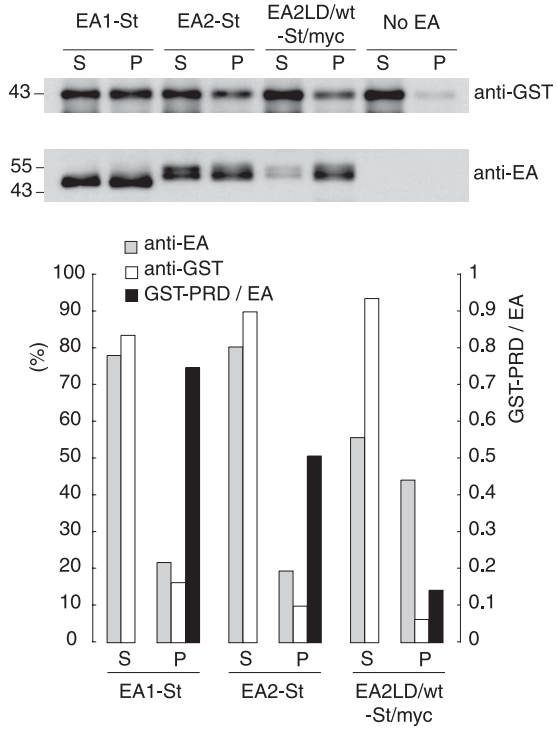

FIGURE 7. **L215D substitution in EA2 reduces SH3 domain-mediated binding of the dynamin PRD by liposome-bound endophilin.** Liposome binding assay was performed by incubating the recombinant PRD of dynamin fused to GST (GST-PRD, 1 μM final concentration) and liposomes in the presence or absence of the indicated endophilins or EA2LD/WT heterodimer for 20 min at 25 °C. Co-sedimentation was determined by SDS-PAGE-Western blot analysis of unbound (supernatant, *S*) and liposome-bound (pellet, *P*) material using GST and endophilin immunoreactivities. Distributions of endophilins and GST-PRD are expressed as a percentage of the respective total material recovered. *Black blocks* represent the ratio of GST-PRD to endophilin in the liposome fraction. In the case of the EA2LD/WT heterodimer, note that the dramatic decrease of the ratio indicates that the mutation in EA2LD strongly impedes PRD recognition by the SH3-domain of bound wild type EA2 endophilins.

shows that residue Leu-215 is localized at the center of a network of stabilizing hydrophobic interactions involving all α-helices of the dimer (Fig. 8*E*).

Expression of EA2LD in Cells Interferes with Endocytic Recycling of the Transferrin Receptor—The incidence of EA2LD expression in HeLa cells was then investigated. First of all, cells were transfected to transiently express EA2 and EA2LD and the respective localization of the two proteins revealed by immunofluorescence. Both proteins were found in the cytosol and, to some extent, at or close to the plasma membrane with a pattern suggestive of small tubular structures (see supplemental Fig. 9). To control the timing and the level of expression of EA2LD, we generated a HeLa/T-Rex stable cell line that expresses EA2LD in a Tet-inducible manner. About 20% of the cell population expressed detectable amounts of the mutant protein already after 5 h of incubation in the presence of 5 μg/ml Tet, which corresponds to 2-fold the endogenous level (Fig. 9*B*). 16 h after Tet induction, the expression level of EA2LD reached 3-fold the endogenous level. The intracellular localization of the protein in Tet-induced HeLa/T-Rex cells appeared similar to the one observed after transfection (Fig. 9*A*, *right panels,* and compare with supplemental Fig. 9). The partial localization of the mutant protein at the plasma membrane suggested that it might be recruited at sites of endocytosis, consistently with the previously described role of endophilin in the endocytic process. To address a possible interfering activity of the BAR mutant in the endocytic pathway, in relation to its abnormal membrane deforming activity, we chose to follow transferrin receptor internalization. HeLa/T-Rex cells were treated or not for 5 and 16 h to induce the expression of EA2LD, followed by a 20-min uptake of Tf-Alexa 563. Because some of the HeLa/T-Rex cells did not seem to express EA2LD in detectable amounts (Fig. 9*A*, *right panel*, cells with delimited area), we also used these cells as internal control, thus preventing potential bias because of Tet treatment. Comparative analysis of Tf-Alexa 568 uptake in EA2LD-expressing and nonexpressing cells revealed, for many of the former, an apparent decrease of Tf-Alexa 563 fluorescence in the recycling endosomes localized in the perinuclear region (Fig. 9*A*, *left*). Using quantitative confocal fluorescence analysis of Tf-Alexa 568 uptake and EA2LD expression, we were able to measure (already after 5 h of Tet induction) a 1.38-fold decrease of uptake in comparison with EA2LD nonexpressing cells present in the same preparation (Fig. 9*C*, *left*). Similar results were obtained after 16 h of Tet induction, with a level of expression not exceeding 1.5-fold that measured after 5 h of Tet induction (Fig. 9*C*, *right*). Altogether, these data complement the results obtained *in vitro* showing alteration of membrane deforming activity of the mutant heterodimer and indicate that EA2LD expressed in cells hampers membrane dynamic events in the endocytic pathway.

DISCUSSION

All BAR domains are spatially organized by the interaction between two protomers that can assemble as homo- or heterodimers and by relatively few residues that are conserved between BAR domain-containing proteins (3). In fact, the signature of this domain, besides its α-helical content, resides in the relatively few amino acid residues that undergo intra- and intermolecular interactions, inside and between monomers. Those residues are mainly of hydrophobic nature (3). Here, we show that the third helix of the BAR sequence of endophilin is capable of dimerization. This is also the case for the first 125 amino acid residues that encompass the first α-helix and part of the second one, as was shown previously (8). This may be significantly different for endophilin B because a two-hybrid interaction assay showed that helix α2 is the most essential for dimerization (23), indicating that the assembly properties of both endophilin A and B members may be significantly different. In agreement with amino acid residues present at the protomer interface (13), we identified leucine 215 as a central residue in dimerization. We show here that this residue is essential for stabilizing hydrophobic interactions between protomers in both EA1 and EA2 homodimers and that its substitution by a negatively charged residue drastically diminishes the interaction between adjacent α3-helices. More importantly, this substitution impairs quite significantly the apparent affinity of full-length endophilin A monomers. To our knowledge, this is the first study reporting on a single point mutagenesis in the BAR sequence that significantly destabilizes the interaction between BAR monomers.

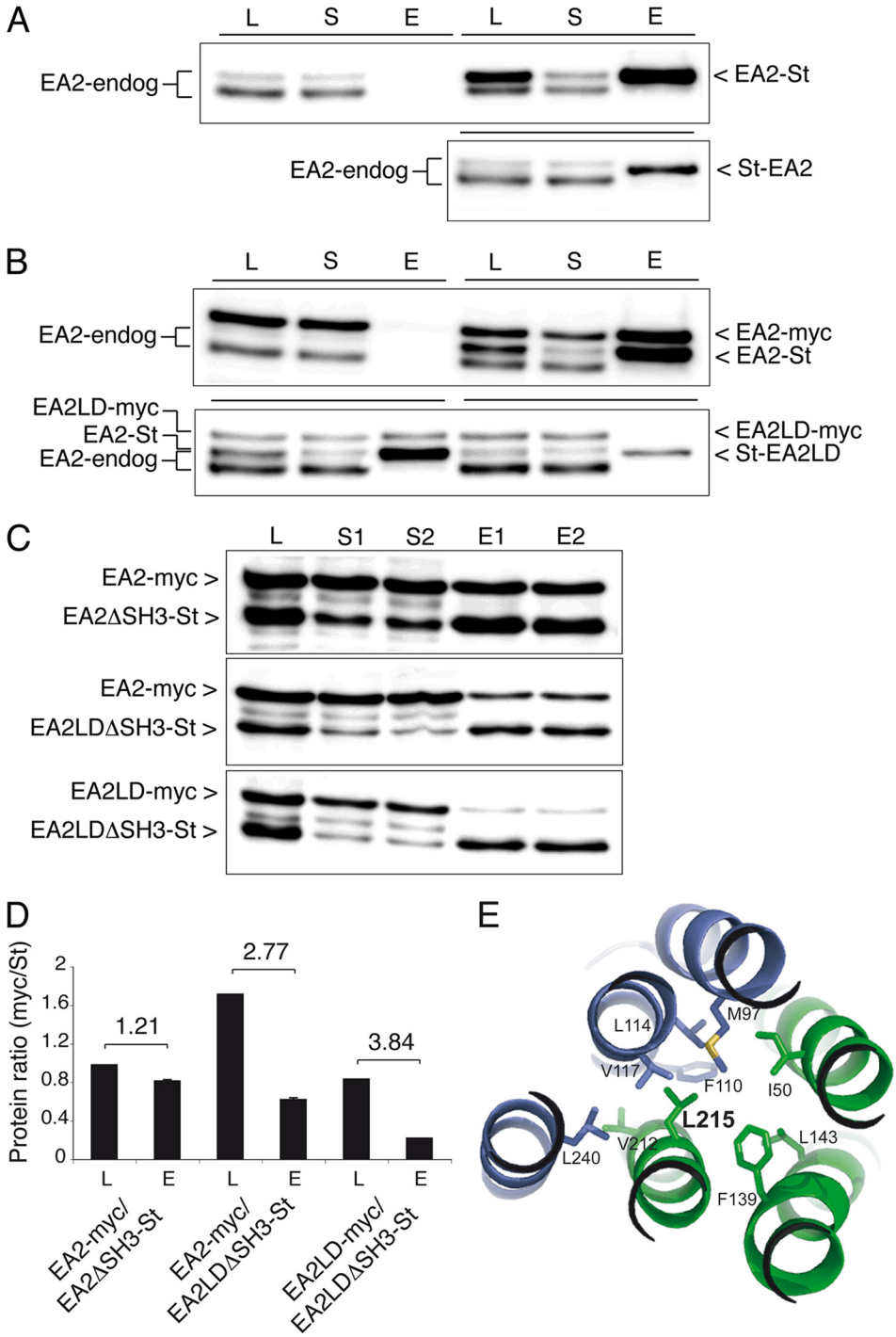

FIGURE 8. **Leucine 215 is a central residue involved in full-length BAR dimerization.** *A–D,* HeLa cells were transfected to express, or co-express, the indicated N- or C-terminal myc and StrepTag (*St*) EA2 fusion proteins (full-length and ΔSH3 ones) and measure their ability to interact either with endogenous EA2 (*EA2-endog*, *A*) or with each other (*B* and *C*) by co-precipitation on StrepTactin/Sepharose. The different epitope-tagged EA2 versions (varying in their respective molecular weights) were analyzed in cell lysates (*L*), StrepTactin/Sepharose supernatants (*S*), and eluates (*E*) by immunoblotting using a polyclonal antiserum recognizing the N terminus of EA2. Note that in *A*, the *left panels* (*L*, *S*) correspond to cells transfected with empty vector and show the migration of endogenous EA2 as well as the absence of nonspecific binding on StrepTactin/Sepharose. Note also that in *B*, the *top panels* (*L*, *S*) correspond to cells expressing EA2-myc and used as negative control to show that myc-tagged proteins do not interact with StrepTactin/Sepharose. *C,* lysates were split in two independent samples to perform precipitation assays in duplicate with the corresponding pairs S1/E1 and S2/E2. *D,* chemiluminescence obtained from immunoblots and corresponding to the myc and StrepTag fusion proteins was captured and quantified in *L* and *E* (for *E*, the value represents the mean of signals obtained in *E1* and *E2*). Results were expressed as the ratio of signals of myc to St forms in *L* and *E*, respectively (protein ratio (myc/St)). *Error bar* for each *E* value corresponds to the variation to the mean for E1 and E2. The *numbers* between *black columns* correspond to the L/E ratio for each condition and give an estimation of the respective efficiency of co-precipitation of the two forms present in each lysate. A value close to 1 indicates that the two forms in the lysate can be precipitated with ~1:1 molar ratio, which is the case for wild type EA2 monomers not bearing the L215D substitution (EA2-myc/EA2ΔSH3-St, L/E ratio = 1.21 and EA2-myc/EA2-St, L/E ratio = 1.14 (not shown)). The highest value obtained for EA2LD dimers (EA2LD-myc/EA2LDΔSH3-St, L/E ratio = 3.84) is in agreement with the significant decrease in affinity between monomers bearing the L215D substitution. *E,* model reconstituted from EA1 BAR domain structure and focusing on the hydrophobic interface built up by residues in the three α-helices of each BAR monomer (each represented in a given color) and localized in the vicinity of residue Leu-215. Note the central location of residue Leu-215 in this network of hydrophobic interactions (W. Weissenhorn, personal communication).

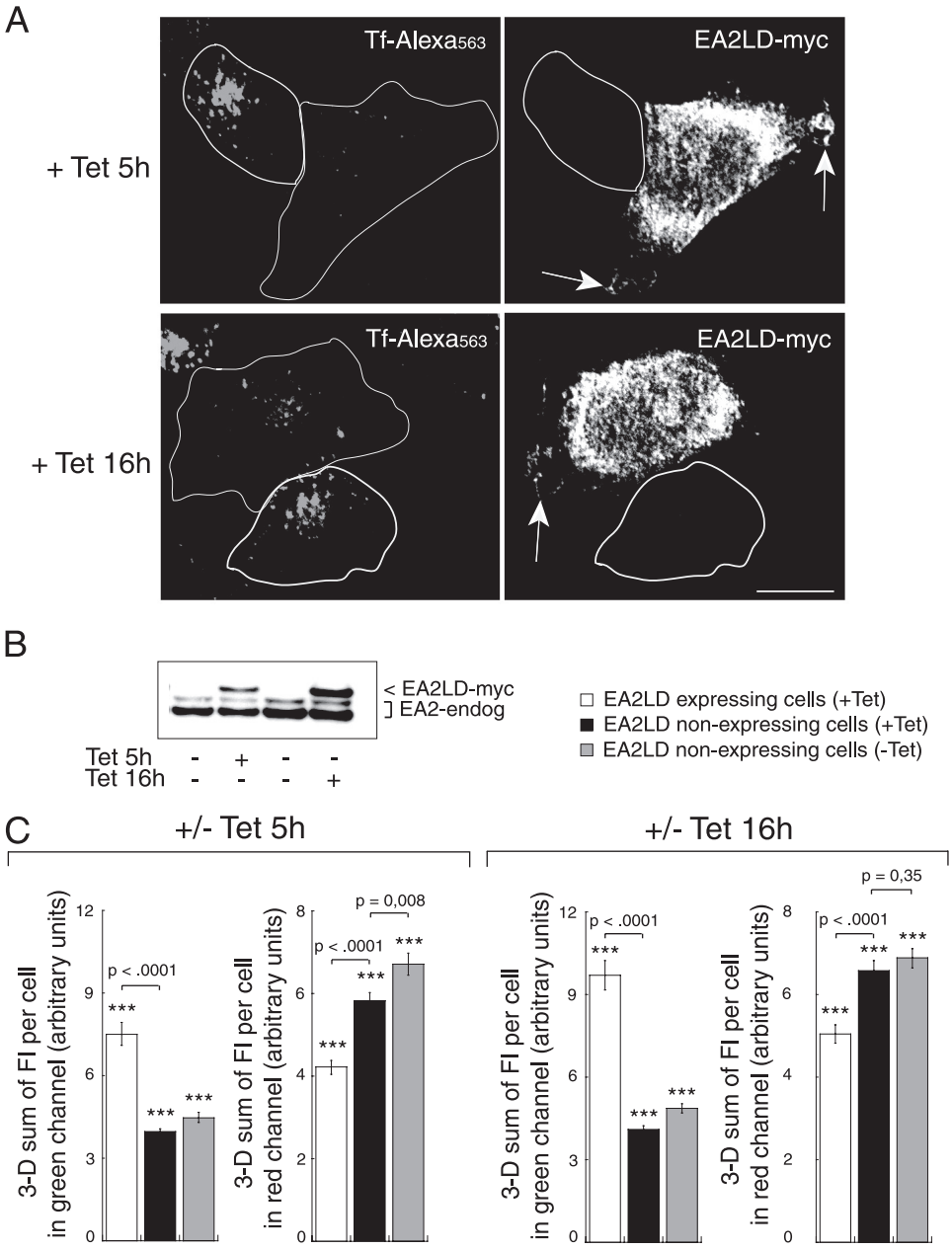

FIGURE 9. **EA2LD expression interferes with transferrin uptake.** HeLa/T-REx cells were treated or not with 5 μg/ml Tet for 5 and 16 h to induce the expression of EA2LD fused to a C-terminal myc tag (EA2LD-myc). *A,* fluorescence microscopy using ApoTome sectioning. After 5 and 16 h of Tet induction, cells were incubated for 20 min in the presence of 10 μg/ml Tf-Alexa 563. Expression of EA2LD was monitored by immunofluorescence using anti-myc primary antibodies and secondary antibodies coupled to Alexa Fluor 488. *Right panels,* EA2LD mainly localizes as an apparent soluble pool in the cytosol as well as on convoluted structures at or beneath the plasma membrane (*arrows*). *Left panels,* comparison between cells that express or not EA2LD of the respective localizations of Tf-Alexa 563 (for quantitative analysis, see *C*). Note, in cells that do not express EA2LD significantly, the accumulation of Tf-Alexa 563 in perinuclear regions corresponding to recycling endosomes as well as the important decrease of signal in this region for cells that express EA2LD. *Bar,* 10 μm. *B,* HeLa/T-REx lysates from cells treated or not with Tet for 5 and 16 h were analyzed by immunoblotting using antibodies recognizing the N terminus of endophilin A. Quantitative analysis of ECL signals corresponding to EA2LD-myc and endogenous EA2 (*EA2-endog*) revealed that EA2LD was expressed ~2- and 3-fold above endogenous level, after 5 and 16 h of Tet induction, respectively. This calculation takes into account that ~20% of cells express the mutant above background (see quantitative analysis of fluorescence in *C*). *C,* quantitative analysis of EA2LD-myc expression levels and fluorescent transferrin (*Tf*) uptake. After treatment or not with Tet (+/−*Tet*), HeLa/T-REx cells were incubated in the presence of Tf-Alexa 563 and processed for immunofluorescence as in *A*. Series of contiguous confocal Z-sections of images, including the entire cellular volume, were captured at emission wavelength of each fluorophore (see "Experimental Procedures"). Fluorescence intensities integrated in the entire volume of each cell (three-dimensional sum of fluorescence intensities per cell) in a given field and for both red and green channels were measured using IMARIS software. Three categories of cells were analyzed as follows: cells not treated with Tet (EA2LD nonexpressing cells (−*Tet*)); cells treated with Tet but for which the fluorescence in the green channel is in the range of the background measured from nontreated cells (EA2LD nonexpressing cells (+*Tet*)), and cells treated with Tet but for which the fluorescence in the green channel is above fluorescence background (EA2LD expressing cells (+*Tet*)). This quantitative analysis revealed that the expression level of EA2LD, after 16 h of Tet induction, corresponds to 1.35-fold that measured after 5 h (compare *white boxes* of *left plots* at 5 and 16 h +/− Tet induction, green channel), which is in agreement with results obtained from immunoblots in *B*. Note that the values in the green channel obtained from EA2LD nonexpressing cells (*black* and *gray boxes*) correspond to background. Note the small but quite significant decrease, at 5 and 16 h +/−Tet induction, of Tf uptake (red channel) by cells that express EA2LD (*white boxes*) in comparison with the internal control condition (*black boxes*). $n = 240$ and 210 cells for EA2LD expressing cells (+*Tet*); $n = 429$ and 275 cells for EA2LD nonexpressing cells (+*Tet*); $n = 237$ and 204 cells for EA2LD nonexpressing cells (−*Tet*), each one of the two values per condition corresponding to cells treated for 5 or 16 h, respectively. *p* values were obtained from Student's *t* test. *** indicates *p* values < 0.0001.

The results presented in this study are all consistent with the requirement of BAR-mediated dimerization for controlling the binding efficiency of the partners of the SH3 domain of endophilin. The strongest evidence in favor of this idea relies on our observation that the SH3 domain of EA1, flanked or not by the variable region, binds poorly to poly-L-proline in comparison with EA1Δ(1–175) that retains α3, the variable region, and the SH3 domain. Indeed, dimer formation by EA1Δ(1–175) in solution necessarily depends on α3 physicochemical properties because the SH3 domain of endophilin does not dimerize (42). However, the observation that EA1 interacts less efficiently with poly-L-proline than EA1Δ(1–175) may be, at first glance, at odds with this hypothesis because full-length BAR monomers can dimerize. Among the two possibilities that have been explored to clarify this apparent inconsistency, (i) the masking of the SH3 domain binding site via intra- or intermolecular interaction with the peptide (^{171}KKKR^{174}) as has been proposed for syndapin and amphiphysin (39) and (ii) the higher propensity of EA1Δ(1–175) to form dimers in solution, the latter one is the most probable. As a matter of fact, neither the mutagenesis of the KKKR peptide in full-length EA1 nor the presence of this peptide at the N terminus of EA1Δ(1–175) changed significantly the interaction with poly-L-proline (which should have been expected if the SH3 domain accessibility to polyproline had been prevented by the peptide). Thus, our results suggest that the KKKR peptide in endophilin A is not functionally equivalent in regulating SH3 domain accessibility to the KKMK sequence of syndapin or to the KKKV sequence of amphiphysin, as proposed by Rao *et al.* (39). In addition, we observed that full-length EA1 is able to transform spherical liposomes into tubules (as opposed to syndapin that, *in vitro* at least, requires a deletion of the SH3 domain to be able to efficiently tubularize membranes). This suggests that a putative regulatory activity of the SH3 domain by masking the KKKR peptide that is clearly involved in membrane binding remains questionable in the case of endophilins. On this line, it should be noticed that the spatial organization of the SH3 domain and the KKKR peptide (localized at the tip of the BAR domain) in endophilin raise the question as to how their interaction can occur within a free dimer (cis-interaction) or in a membrane-bound oligomer (trans-interaction). In this respect, it should be noted that the tetrapeptides in amphiphysin (KKKV) and in syndapin 1 (KKMK) have a more proximal position relatively to the C terminus of helix 3 in the BAR domain and that the polypeptide linker between the BAR/F-BAR and the SH3 domain is 382 and 75 amino acid residues long in amphiphysin and syndapin 1, respectively, as compared with 41 amino acid residues in endophilin. Hence, for the latter, this might contribute to restrict the accessibility of the SH3 domain to the KKKR sequence.

Finally and regarding the apparent lower capacity of EA1 to interact with poly-L-proline, this can be explained by the fact that the affinity of full-length BAR monomers may be significantly lower than that of α3-helices. This implies that EA1 would be present predominantly in the monomeric form upon bacterial synthesis and in the bacterial supernatants prepared for affinity chromatography, in agreement with the estimated dimerization constant of endophilin A N-BAR sequences (5–15 μM range) (9, 46). Consistently, we have estimated that the maximum endophilin concentration in bacterial lysates is below 1 μM. In addition, this is also consistent with our data showing that, in solution and in the presence of equal concentration of cross-linking agent, full-length EA1 forms less dimers in comparison with EA1Δ(1–175).

In the course of characterizing the incidence of the L215D substitution on the function of endophilin in membrane binding and deformation, we made several unexpected observations leading to challenging interpretations. Upon incubation of the EA2LD/WT heterodimer with liposomes, we observed a very significant increase in the binding of both wild type and mutant forms, in comparison with the condition in which wild type EA2 was used. This implies that a BAR domain made of wild type and mutant protomers exhibits functional properties different from wild type. Heterodimers represent sites of loose protomer-protomer interactions. Thus, besides a possible dissociation of mutant BAR after binding that should destabilize oligomers, an altered function at/on the membrane may result essentially from a decreased rigidity of the molecule. This may modify the stringency of the BAR regarding the curvature index of the membrane onto which it assembles. This may have two consequences that would, most probably, result in the improved membrane binding as follows: (i) increase the surface capacity of membranes onto which the BAR can be recruited because a lower rigidity would allow binding to vesicles of larger diameter (although liposomes were extruded, dispersion of their size remains significant) and (ii) decrease of the off-rate from membranes in a scenario where the rigidity of the wild type BAR domain triggers release from membranes when the curvature index has reached a lower limit. The morphology of the structures that we observed by electron microscopy after incubation of the mutant heterodimer with liposomes may be consistent, at least in part, with these interpretations. First, in addition to membrane tubules of altered shape, clusters of spheres with diameters ranging from 100 to 300 nm were seen. These may account for a population of liposomes at the surface of which mutant heterodimers are recruited but that cannot be deformed into tubules. Second, the tubules of irregular shape and diameter that were formed are characterized by constrictions of very narrow diameter. These may result from the decrease in rigidity of the mutant BAR domain that cannot stabilize the diameter of the tube to the one that would be imposed by the intrinsic curvature radius of a wild type BAR domain (or of that imposed by wild type BAR oligomers). On this line, it should be noticed that the quite significant increase in the number of small spherical particles may result from the instability (and subsequent fission) generated by the presence of mutant heterodimers on membranes of narrow diameter.

In conclusion, this work brings novel insights into the functional relationship between the two structural units that build up proteins of the endophilin A subfamily, the BAR and the flanking SH3 domains. With the help of point mutagenesis of a residue that plays a central role on stabilizing interactions between BAR protomers, we confirm the critical role of the BAR conformation and rigidity in exerting stringent control on membrane curvature and, which has been poorly investigated until now, the binding efficiency of partners of the SH3 domain

(in the case of endophilins at least). It should be noticed that quite recently Wong *et al*. (47) have reported on the regulation of BAR sequence dimerization of endophilin B1 by Cdk-5-dependent phosphorylation leading to an increase in the recruitment of UV radiation resistance-associated gene protein for subsequent activation of autophagy. Therefore, our findings would support the emerging notion that the BAR sequence self-assembly critically functions as a signal for recruitment of downstream effectors of proteins of the endophilin family. Finally, BAR-mediated dimerization has also been reported to be required for Sorting Nexin 9 to interact with the kinase ACK2 (activated Cdc42-associated tyrosine kinase 2) thereby triggering the degradation of epidermal growth factor receptor (48).

Acknowledgments—We thank W. Weissenhorn for helpful discussions and ultrastructural modeling analysis and X. Baudin and V. Contremoulins for technical support on quantitative fluorescence analysis.

REFERENCES

1. Frost, A., Unger, V. M., and De Camilli, P. (2009) The BAR domain superfamily. Membrane-molding macromolecules. *Cell* **137,** 191–196
2. Tarricone, C., Xiao, B., Justin, N., Walker, P. A., Rittinger, K., Gamblin, S. J., and Smerdon, S. J. (2001) The structural basis of Arfaptin-mediated cross-talk between Rac and Arf signaling pathways. *Nature* **411,** 215–219
3. Peter, B. J., Kent, H. M., Mills, I. G., Vallis, Y., Butler, P. J., Evans, P. R., and McMahon, H. T. (2004) BAR domains as sensors of membrane curvature. The amphiphysin BAR structure. *Science* **303,** 495–499
4. Frost, A., Perera, R., Roux, A., Spasov, K., Destaing, O., Egelman, E. H., De Camilli, P., and Unger, V. M. (2008) Structural basis of membrane invagination by F-BAR domains. *Cell* **132,** 807–817
5. Saarikangas, J., Zhao, H., Pykäläinen, A., Laurinmäki, P., Mattila, P. K., Kinnunen, P. K., Butcher, S. J., and Lappalainen, P. (2009) Molecular mechanisms of membrane deformation by I-BAR domain proteins. *Curr. Biol.* **19,** 95–107
6. Wang, Q., Kaan, H. Y., Hooda, R. N., Goh, S. L., and Sondermann, H. (2008) Structure and plasticity of endophilin and sorting nexin 9. *Structure* **16,** 1574–1587
7. Mattila, P. K., Pykäläinen, A., Saarikangas, J., Paavilainen, V. O., Vihinen, H., Jokitalo, E., and Lappalainen, P. (2007) Missing-in-metastasis and IRSp53 deform PI(4,5)P_2-rich membranes by an inverse BAR domain-like mechanism. *J. Cell Biol.* **176,** 953–964
8. Farsad, K., Ringstad, N., Takei, K., Floyd, S. R., Rose, K., and De Camilli, P. (2001) Generation of high curvature membranes mediated by direct endophilin bilayer interactions. *J. Cell Biol.* **155,** 193–200
9. Gallop, J. L., Jao, C. C., Kent, H. M., Butler, P. J., Evans, P. R., Langen, R., and McMahon, H. T. (2006) Mechanism of endophilin N-BAR domain-mediated membrane curvature. *EMBO J.* **25,** 2898–2910
10. Masuda, M., Takeda, S., Sone, M., Ohki, T., Mori, H., Kamioka, Y., and Mochizuki, N. (2006) Endophilin BAR domain drives membrane curvature by two newly identified structure-based mechanisms. *EMBO J.* **25,** 2889–2897
11. Bhatia, V. K., Madsen, K. L., Bolinger, P. Y., Kunding, A., Hedegård, P., Gether, U., and Stamou, D. (2009) Amphipathic motifs in BAR domains are essential for membrane curvature sensing. *EMBO J.* **28,** 3303–3314
12. Madsen, K. L., Bhatia, V. K., Gether, U., and Stamou, D. (2010) BAR domains, amphipathic helices, and membrane-anchored proteins use the same mechanism to sense membrane curvature. *FEBS Lett.* **584,** 1848–1855
13. Weissenhorn, W. (2005) Crystal structure of the endophilin-A1 BAR domain. *J. Mol. Biol.* **351,** 653–661
14. Jao, C. C., Hegde, B. G., Gallop, J. L., Hegde, P. B., McMahon, H. T., Haworth, I. S., and Langen, R. (2010) Roles of amphipathic helices and the bin/amphiphysin/rvs (BAR) domain of endophilin in membrane curvature generation. *J. Biol. Chem.* **285,** 20164–20170
15. Kjaerulff, O., Brodin, L., and Jung, A. (2011) The structure and function of endophilin proteins. *Cell Biochem. Biophys.* **60,** 137–154
16. Sparks, A. B., Hoffman, N. G., McConnell, S. J., Fowlkes, D. M., and Kay, B. K. (1996) Cloning of ligand targets. Systematic isolation of SH3 domain-containing proteins. *Nat. Biotechnol.* **14,** 741–744
17. Giachino, C., Lantelme, E., Lanzetti, L., Saccone, S., Bella Valle, G., and Migone, N. (1997) A novel SH3-containing human gene family preferentially expressed in the central nervous system. *Genomics* **41,** 427–434
18. de Heuvel, E., Bell, A. W., Ramjaun, A. R., Wong, K., Sossin, W. S., and McPherson, P. S. (1997) Identification of the major synaptojanin-binding proteins in brain. *J. Biol. Chem.* **272,** 8710–8716
19. Ringstad, N., Nemoto, Y., and De Camilli, P. (1997) The SH3p4/Sh3p8/SH3p13 protein family. Binding partners for synaptojanin and dynamin via a Grb2-like Src homology 3 domain. *Proc. Natl. Acad. Sci. U.S.A.* **94,** 8569–8574
20. Micheva, K. D., Ramjaun, A. R., Kay, B. K., and McPherson, P. S. (1997) SH3 domain-dependent interactions of endophilin with amphiphysin. *FEBS Lett.* **414,** 308–312
21. Huttner, W. B., and Schmidt, A. (2000) Lipids, lipid modification, and lipid-protein interaction in membrane budding and fission. Insights from the roles of endophilin A1 and synaptophysin in synaptic vesicle endocytosis. *Curr. Opin. Neurobiol.* **10,** 543–551
22. Cuddeback, S. M., Yamaguchi, H., Komatsu, K., Miyashita, T., Yamada, M., Wu, C., Singh, S., and Wang, H. G. (2001) Molecular cloning and characterization of Bif-1. A novel Src homology 3 domain-containing protein that associates with Bax. *J. Biol. Chem.* **276,** 20559–20565
23. Pierrat, B., Simonen, M., Cueto, M., Mestan, J., Ferrigno, P., and Heim, J. (2001) SH3GLB, a new endophilin-related protein family featuring an SH3 domain. *Genomics* **71,** 222–234
24. Ringstad, N., Gad, H., Löw, P., Di Paolo, G., Brodin, L., Shupliakov, O., and De Camilli, P. (1999) Endophilin/SH3p4 is required for the transition from early to late stages in clathrin-mediated synaptic vesicle endocytosis. *Neuron* **24,** 143–154
25. Schmidt, A., and Huttner, W. B. (1998) Biogenesis of synaptic-like microvesicles in perforated PC12 cells. *Methods* **16,** 160–169
26. Gad, H., Ringstad, N., Löw, P., Kjaerulff, O., Gustafsson, J., Wenk, M., Di Paolo, G., Nemoto, Y., Crun, J., Ellisman, M. H., De Camilli, P., Shupliakov, O., and Brodin, L. (2000) Fission and uncoating of synaptic clathrin-coated vesicles are perturbed by disruption of interactions with the SH3 domain of endophilin. *Neuron* **27,** 301–312
27. Guichet, A., Wucherpfennig, T., Dudu, V., Etter, S., Wilsch-Bräuniger, M., Hellwig, A., González-Gaitán, M., Huttner, W. B., and Schmidt, A. A. (2002) Essential role of endophilin A in synaptic vesicle budding at the *Drosophila* neuromuscular junction. *EMBO J.* **21,** 1661–1672
28. Verstreken, P., Kjaerulff, O., Lloyd, T. E., Atkinson, R., Zhou, Y., Meinertzhagen, I. A., and Bellen, H. J. (2002) Endophilin mutations block clathrin-mediated endocytosis but not neurotransmitter release. *Cell* **109,** 101–112
29. Rikhy, R., Kumar, V., Mittal, R., and Krishnan, K. S. (2002) Endophilin is critically required for synapse formation and function in *Drosophila melanogaster*. *J. Neurosci.* **22,** 7478–7484
30. Schuske, K. R., Richmond, J. E., Matthies, D. S., Davis, W. S., Runz, S., Rube, D. A., van der Bliek, A. M., and Jorgensen, E. M. (2003) Endophilin is required for synaptic vesicle endocytosis by localizing synaptojanin. *Neuron* **40,** 749–762
31. Wan, J., Cheung, A. Y., Fu, W. Y., Wu, C., Zhang, M., Mobley, W. C., Cheung, Z. H., and Ip, N. Y. (2008) Endophilin B1 as a novel regulator of nerve growth factor/TrkA trafficking and neurite outgrowth. *J. Neurosci.* **28,** 9002–9012
32. Karbowski, M., Jeong, S. Y., and Youle, R. J. (2004) Endophilin B1 is required for the maintenance of mitochondrial morphology. *J. Cell Biol.* **166,** 1027–1039
33. Takahashi, Y., Karbowski, M., Yamaguchi, H., Kazi, A., Wu, J., Sebti, S. M., Youle, R. J., and Wang, H. G. (2005) Loss of Bif-1 suppresses Bax/Bak conformational change and mitochondrial apoptosis. *Mol. Cell. Biol.* **25,** 9369–9382

34. Etxebarria, A., Terrones, O., Yamaguchi, H., Landajuela, A., Landeta, O., Antonsson, B., Wang, H. G., and Basañez, G. (2009) Endophilin B1/Bif-1 stimulates BAX activation independently from its capacity to produce large scale membrane morphological rearrangements. *J. Biol. Chem.* **284,** 4200–4212
35. Rostovtseva, T. K., Boukari, H., Antignani, A., Shiu, B., Banerjee, S., Neutzner, A., and Youle, R. J. (2009) Bax activates endophilin B1 oligomerization and lipid membrane vesiculation. *J. Biol. Chem.* **284,** 34390–34399
36. Takahashi, Y., Coppola, D., Matsushita, N., Cualing, H. D., Sun, M., Sato, Y., Liang, C., Jung, J. U., Cheng, J. Q., Mulé, J. J., Pledger, W. J., and Wang, H. G. (2007) Bif-1 interacts with Beclin 1 through UVRAG and regulates autophagy and tumorigenesis. *Nat. Cell Biol.* **9,** 1142–1151
37. Yang, J. S., Zhang, L., Lee, S. Y., Gad, H., Luini, A., and Hsu, V. W. (2006) Key components of the fission machinery are interchangeable. *Nat. Cell Biol.* **8,** 1376–1382
38. Loll, P. J., Swain, E., Chen, Y., Turner, B. T., and Zhang, J. F. (2008) Structure of the SH3 domain of rat endophilin A2. *Acta Crystallogr. Sect. F Struct. Biol. Cryst. Commun.* **64,** 243–246
39. Rao, Y., Ma, Q., Vahedi-Faridi, A., Sundborger, A., Pechstein, A., Puchkov, D., Luo, L., Shupliakov, O., Saenger, W., and Haucke, V. (2010) Molecular basis for SH3 domain regulation of F-BAR-mediated membrane deformation. *Proc. Natl. Acad. Sci. U.S.A.* **107,** 8213–8218
40. Schmidt, A., Wolde, M., Thiele, C., Fest, W., Kratzin, H., Podtelejnikov, A. V., Witke, W., Huttner, W. B., and Söling, H. D. (1999) Endophilin I mediates synaptic vesicle formation by transfer of arachidonate to lysophosphatidic acid. *Nature* **401,** 133–141
41. Schmidt, A., Hannah, M. J., and Huttner, W. B. (1997) Synaptic-like microvesicles of neuroendocrine cells originate from a novel compartment that is continuous with the plasma membrane and devoid of transferrin receptor. *J. Cell Biol.* **137,** 445–458
42. Ringstad, N., Nemoto, Y., and De Camilli, P. (2001) Differential expression of endophilin 1 and 2 dimers at central nervous system synapses. *J. Biol. Chem.* **276,** 40424–40430
43. Cestra, G., Castagnoli, L., Dente, L., Minenkova, O., Petrelli, A., Migone, N., Hoffmüller, U., Schneider-Mergener, J., and Cesareni, G. (1999) The SH3 domains of endophilin and amphiphysin bind to the proline-rich region of synaptojanin 1 at distinct sites that display an unconventional binding specificity. *J. Biol. Chem.* **274,** 32001–32007
44. Howard, L., Nelson, K. K., Maciewicz, R. A., and Blobel, C. P. (1999) Interaction of the metalloprotease disintegrins MDC9 and MDC15 with two SH3 domain-containing proteins, endophilin I and SH3PX1. *J. Biol. Chem.* **274,** 31693–31699
45. Lim, K., Ho, J. X., Keeling, K., Gilliland, G. L., Ji, X., Rüker, F., and Carter, D. C. (1994) Three-dimensional structure of *Schistosoma japonicum* glutathione *S*-transferase fused with a six-amino acid conserved neutralizing epitope of gp41 from HIV. *Protein Sci.* **3,** 2233–2244
46. Ross, J. A., Chen, Y., Müller, J., Barylko, B., Wang, L., Banks, H. B., Albanesi, J. P., and Jameson, D. M. (2011) Dimeric endophilin A2 stimulates assembly and GTPase activity of dynamin 2. *Biophys. J.* **100,** 729–737
47. Wong, A. S., Lee, R. H., Cheung, A. Y., Yeung, P. K., Chung, S. K., Cheung, Z. H., and Ip, N. Y. (2011) Cdk5-mediated phosphorylation of endophilin B1 is required for induced autophagy in models of Parkinson disease. *Nat. Cell Biol.* **13,** 568–579
48. Childress, C., Lin, Q., and Yang, W. (2006) Dimerization is required for SH3PX1 tyrosine phosphorylation in response to epidermal growth factor signaling and interaction with ACK2. *Biochem. J.* **394,** 693–698